

LA-UR-17-23974

Approved for public release; distribution is unlimited.

Title: PHELIX Crenulation 2 and 3 Flash Report

Author(s): Rousculp, Christopher L.; Oro, David Michael; Griego, Jeffrey Randall; Patten, Austin Randall; Neukirch, Levi Patrick; Reinovsky, Robert Emil; Turchi, Peter John; Bradley, Joseph Thomas III; Reass, William Allen; Fierro, Franklin; Saunders, Alexander; Mariam, Fesseha Gebre; Freeman, Matthew Stouten; Cheng, Baolian; Tang, Zhaowen

Intended for: Report

Issued: 2017-05-16

Disclaimer:

Los Alamos National Laboratory, an affirmative action/equal opportunity employer, is operated by the Los Alamos National Security, LLC for the National Nuclear Security Administration of the U.S. Department of Energy under contract DE-AC52-06NA25396. By approving this article, the publisher recognizes that the U.S. Government retains nonexclusive, royalty-free license to publish or reproduce the published form of this contribution, or to allow others to do so, for U.S. Government purposes. Los Alamos National Laboratory requests that the publisher identify this article as work performed under the auspices of the U.S. Department of Energy. Los Alamos National Laboratory strongly supports academic freedom and a researcher's right to publish; as an institution, however, the Laboratory does not endorse the viewpoint of a publication or guarantee its technical correctness.

PHELIX Crenulation 2 and 3 Flash Report

C. L. Rousculp, D. M. Oro, J. R. Griego, A. R. Patten, L. P. Neukirch, R. E. Reinovsky, P. J. Turchi, J. T. Bradley, W. A. Reass, F. Fierro, A. Saunders, F. G. Mariam, M. S. Freeman, B. Cheng, Z. Tang – 3 April 2017

Purpose

This report documents the execution of the PHELIX driven Crenulation 2 and 3 at LANSCE proton radiography experiments in FY17 in support of the LANL Science Campaign-1 L2 Milestone (#5721). It should be noted that LANL Science Campaign 3 also supports the PHELIX at pRad efforts.

Background

There is great interest in the behavior of the free surface of tin under shock loading. While it is known that meso-scale surface imperfections can seed the Richtmyer-Meshkov Instability (RMI) for a surface that is melted on release, much less is known about a tin surface that is solid, but plastically deforming. Here material properties such as shear and yield strength come into play especially in converging geometry.

Previous experiments have been driven by direct contact HE. Usually a thin, flat target coupon is fielded with various single-mode, sinusoidal, machined, profiles on the free surface. The free surface is adjacent to either vacuum or an inert receiver gas. Most of these previous driver/target configurations have been nominal planer geometry. With modern HE it has been straightforward to shock tin into melt on release. However it has been challenging to achieve a low enough pressure for solid state on release.

Here we propose to extend the existing base of knowledge to include the behavior of the free surface of tin in cylindrical converging geometry. By shock loading a cylindrical tin shell with a magnetically driven cylindrical liner impactor, the free surface evolution can be diagnosed with proton radiography. With the PHELIX capacitor bank, the drive can easily be varied to span the pressure range to achieve solid, mixed, and liquid states on release. A conceptual cylindrical liner and target is shown in Figure 1.

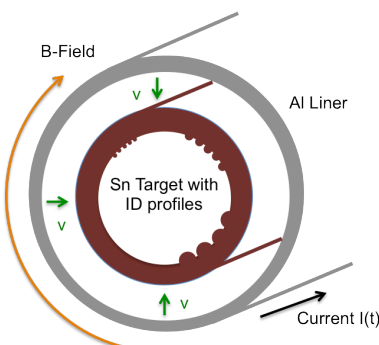


Figure 1. Conceptual cylindrical and target. The target has three different single-mode flute profiles on the inner surface.

Motivation

Current computational modeling paradigms of ejectaⁱ are broken down into production, transport, and evolution. The production model is based on characteristic surface roughness and material phase. When a fluid, non-smooth surface is subject to shock, the RMI produces spikes of material that can be ejected from the surface. This model has been verified and quantified in an extensive series of experiments where single mode initial surface perturbations were subject to HE shock loading and melt on release^{ii,iii}. Proton radiography imaged nonlinear amplitude growth and piezo pins measured total ejected mass as a function of time. However, one shortcoming of these HE driven experiments is that the drive is fixed and it is difficult to shock a tin sample such that it is solid on release. Thus a variable drive method that could span the range of pressures for release into solid, mixed, or fluid state would be highly valuable.

Recent theoretical work on the EOS of tin has modified both the Hugoniot and the isentropes for release into various states in tabular data. The new multiphase EOS for tin, SESAME 2161, includes the beta and gamma solid phases as well as a liquid phase. It predicts a lower pressure boundary for release to pure solid (~20 GPa) and a higher-pressure boundary for release to pure liquid (~35 GPa) than the existing SESAME 2160 table. Seen in Figure 2, is a phase space comparison of the two tables^{iv}. Experimentally, the new table requires a much broader range of accessible pressure drive to validate.

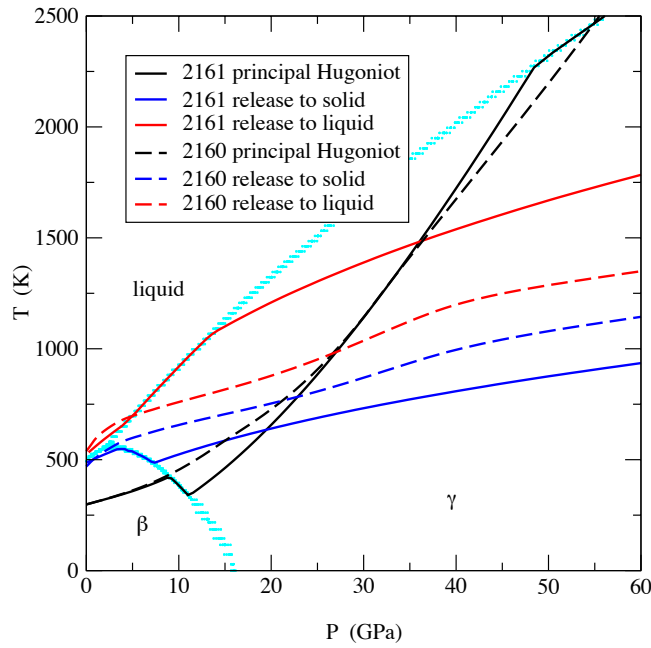


Figure 2. Phase diagram comparing multiphase SESAME 2161 with 2160.

Also under development in the ASC Lagrangian Applications Project (LAP) Flag code is a multi-phase material model that is phase-aware. There, a Steinberg-Guinan strength model is applied with separate parameters to the beta and gamma phases while the liquid phase is strengthless.^v

The main technique for the study of RMI growth and validation of models has been single-mode sinusoidal profile of a planer tin surface. However, if a similar profile is imposed on the inside of a cylinder, it is not as clear what the mechanism for amplitude growth might be when the cylinder is driven radially inward. On the one hand, if conservation of cylindrical solid area is assumed, then for constant velocity, amplitude growth can be shown to be proportional to $t^{1/2}$. However, if conservation of cylindrical fluid mass is assumed then the amplitude at early time grows linearly as

$$A(t) \approx A_0(1 + \frac{vt}{R_0})$$

Here, R_0 is the initial cylinder radius; v is the surface's radial velocity. Note that it is independent of the mode number of the perturbation^{vi}.

Magnetic Pulsed-Power Hydrodynamics

For these experiments the Precision High Energy-density Liner Implosion Experiment (PHELIX) portable capacitor bank will be utilize. PHELIX is a 300 kJ capacitor bank located at the LANL LANSCE proton radiography facility. It is capable of delivering a 4 MA, 10 μ s current pulse to a low inductance cylindrical load. A picture of PHELIX at pRad is shown in Figure 3.



Figure 3. PHELIX at pRad.

PHELIX was designed to achieve the same velocities and pressures as larger capacitor systems by scaling down in size liner-on-target experiments and requiring less stored energy^{vii}.

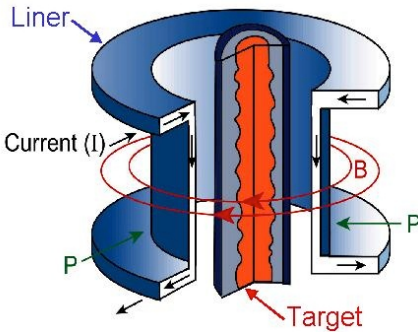


Figure 4. Schematic of a magnetically driven, liner-on-target experiment.

A general, magnetically driven, cylindrical liner-on-target, shock experiment is shown in Figure 4. For an axial directed current, I , passing through a liner of radius, R , an azimuthal directed magnetic field, B , produces a driving pressure given by,

$$P = \frac{\mu_0 I^2}{8\pi^2 R^2}$$

Thus, the same drive pressure can be achieved by keeping the ratio of I/R constant. By utilizing PHELIX with pRad (instead of traditional 4-frame flash X-ray imaging), a high-quality, high data rate can be achieved per experiment in an economical fashion.

Results of Crenulation-1

The first in this series of experiments was conducted in December of 2015. A 3 cm diameter Al liner and a 1 cm diameter tin target was fielded. For this experiment both the region between the liner/target and the region inside the target were evacuated to few mTorr. A cutaway view of the liner-on-target system is shown in Figure 5.

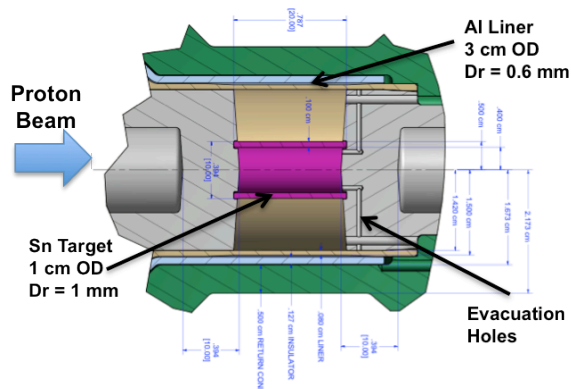


Figure 5. Cutaway view of the Crenulation-1 liner-on-target system.

The ID of the tin target was divided into three 120-degree sectors. Each sector had a single-mode perturbation of wavelength 1.10 mm machined into the surface with \sim 60-degrees of unperturbed surface between. The amplitude of the perturbation varied to give a wavelength/amplitude product, kA = 0.1, 0.2, and 0.3. A surface finish of 3.57/21.91 micro-in on the OD/ID of the target was achieved. Detail of the layout is shown in Figure 6.

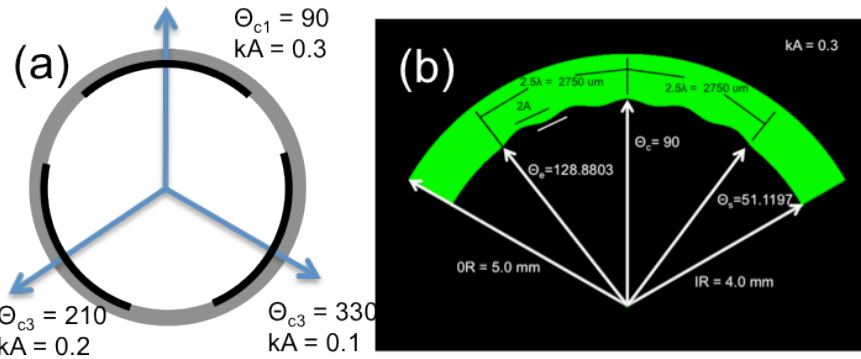


Figure 6. (a) Three sector layout of the ID of the tin target. (b) Details of the $kA = 0.3$ sector.

The images have been analyzed and the growth of the $kA = 0.3$ sector has been compared to calculations. Figure 7 shows calculations and a comparison to the data. Good agreement is seen and the amplitude appears linear in time. This is consistent with the theory of conservation of shell volume. Also, it should be noted that in the calculation at late times, a density depression (cavitation) due layer is observed near the OD of the target. This is indicated by dark blue at $T = 9.0$ μs in Figure 7.

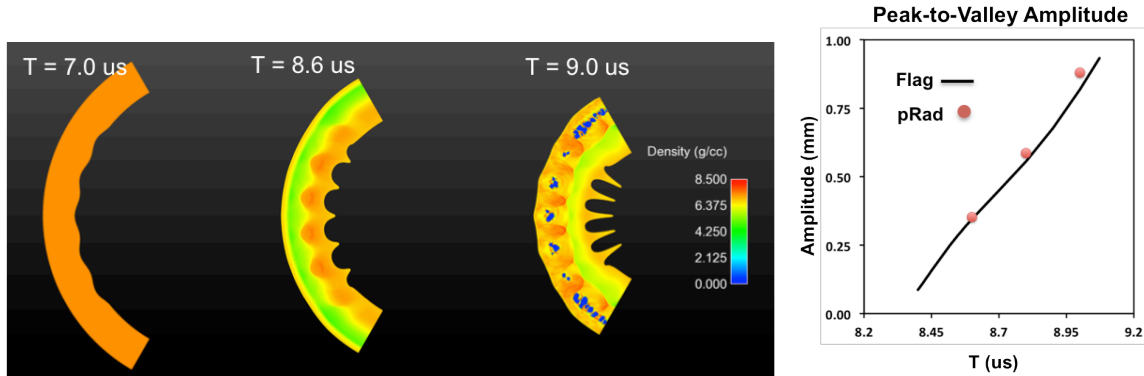
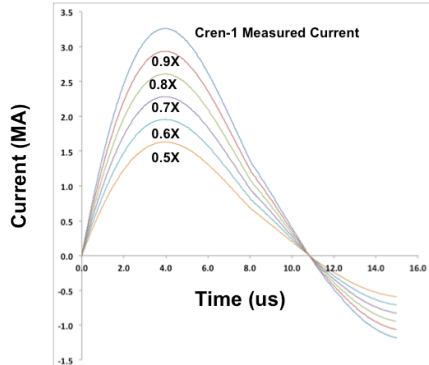


Figure 7. Flag calculation of the $kA = 0.3$ sector and a comparison to the data.

PHELIX Crenulation 2 and 3 - Computational Study of Release to Mixed and Solid States

Prior to the experiment execution, a computational study was undertaken to determine the necessary PHELIX drive parameters to individually shock the tin cylinder to a mixed state on release and a solid state on release. A series of calculations was performed in which the measured current is fractionally scaled. This is a feature readily achievable by with pulsed power, but difficult with HE drive. Figure 8 shows both the scaled load current profiles used in simulations and the resulting liner velocity, shock velocity, and shock pressure.



Scale Factor	Liner Velocity (km/s)	V_shock in Tin (km/s)	P_shock in Tin (Gpa)
1	2.9	1	38
0.9	2.1	0.9	29
0.8	1.5	0.8	20
0.7	1.3	0.65	14
0.6	1	0.4	9.5
0.5	0.74	0.3	7.3

Figure 8. (Left) Fractional scaling of the load current used in simulations. (Right) Drive parameter from the simulations.

I = 0.8x Case

The 0.8x case is interesting for two reasons. First, as the spikes release into the liquid phase, but at late time the tips refreeze into the beta phase where strength traps the advancing liquid and causes blunting of the tip. Second, the bubbles release to solid, but under compression from convergence end up in the liquid state and develop a secondary structure. The calculation is shown in Figure 9 with the left being colored by density and the right being colored by dominant phase in a cell. Finally, the velocities of the spike and bubble show that the spike profile is the same as in the $I = 1.0x$ case, the bubble actually experiences a strong acceleration under convergence and had a greater velocity than then spike when the calculation terminates due to mesh tangling. The velocity profiles are shown in Figure 10. It should be kept in mind that that while the model includes multiphase EOS and phase aware strength; it does not include surface tension.

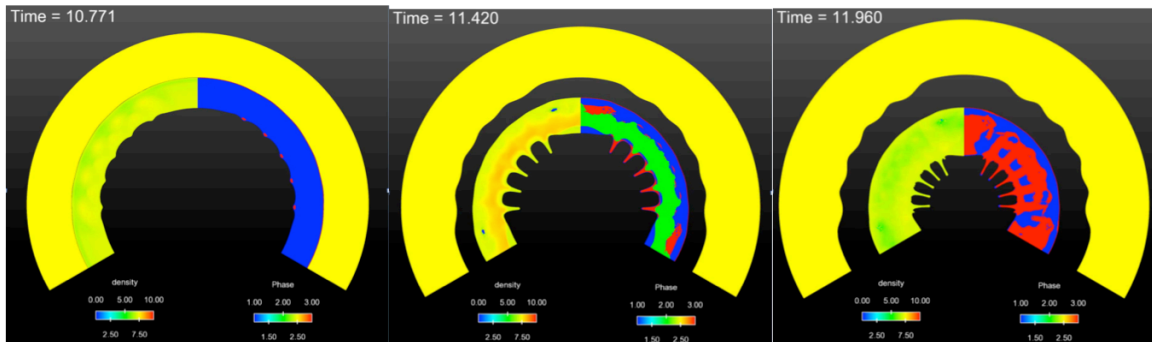


Figure 9. $I = 0.8X$, $kA = 0.3$ simulation. Spike release to liquid (red) but have their tips refreeze into the beta phase (blue) causing blunting at late time. The bulk transitions from beta to gamma (green) and liquid.

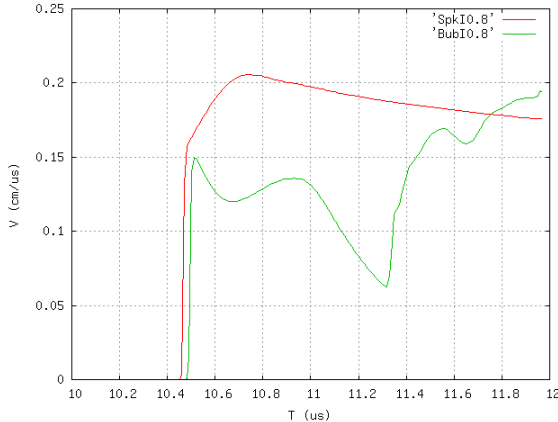


Figure 10. Spike and bubble velocities for $I = 0.8x$, $kA = 0.3$ calculation.

$I = 0.6x$ Case

By reducing the drive even further, the tin target can be made to remain in the beta phase throughout the implosion. The single-mode perturbation still inverts under RMI, but the amplitude growth is suppressed by material strength. Shown in Figure 11 are the initial and final states of the single-mode perturbation in the calculation.

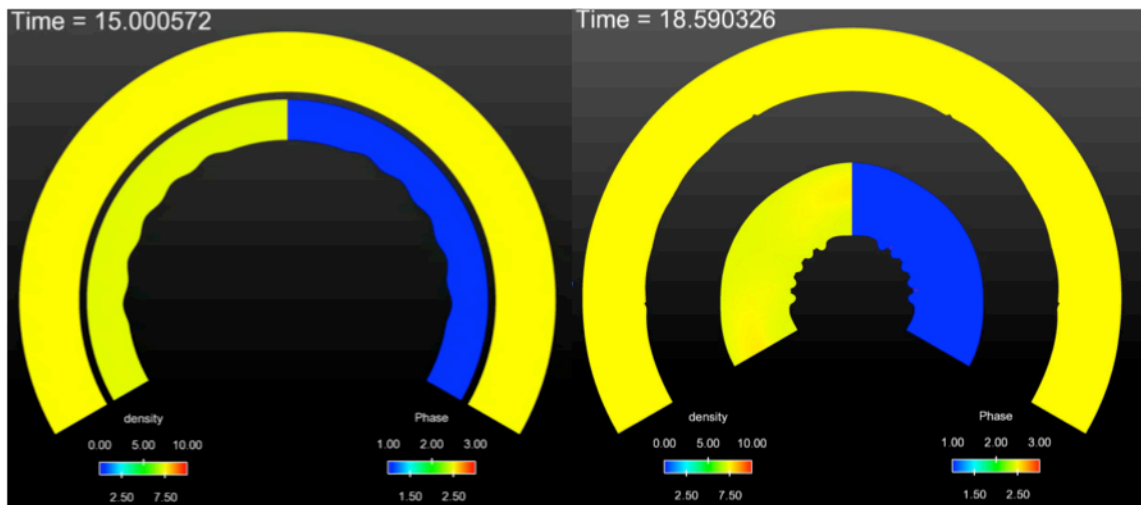


Figure 11. $I = 0.6x$, $kA = 0.3$ calculation before impact and when the calculation terminates.

Looking at the velocities of the spike and bubble in Figure 12, the transit time reflections of shocks between the inner and outer surfaces becomes apparent. This causes the interesting effect of the bubble moving faster than the spike, which means the amplitude is shrinking under convergence. This leads to the question that if a shell of the same thickness but with an initially larger radius, were driven at the same shock pressure, would the perturbation amplitude go to zero?

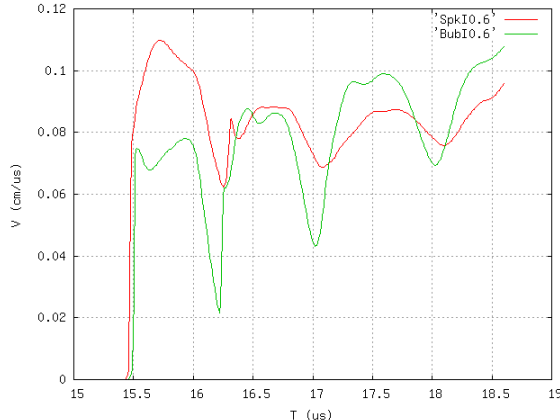


Figure 12. Spike and bubble velocity profiles for the $I = 0.6x$, $kA = 0.3$ case. Note at late time the bubble velocity is greater than the spike.

New PHELIX Load to Beam Pipe System

Due to axial jetting in the Cren-1 experiment in FY16, a new confinement system was designed to couple the PHELIX load cassette directly to the pRad beam pipes. This replaces the original air gap system. The system utilized shielded vacuum bellows to facilitate high-precision alignment as well as dielectric stand-offs for electrical isolation. Figure 15 shows a schematic of the new system with the liner and target.

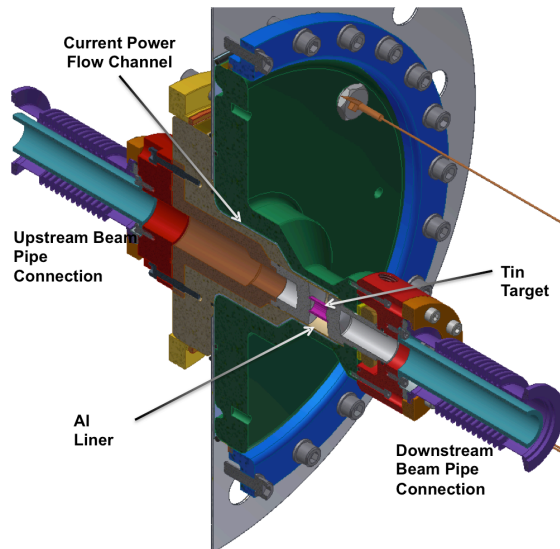


Figure 13. PHELIX Crenulation load cassette with new beam pipe connections.

Experimental Results

The data include measured drive current from optical Faraday rotation diagnostic. Figure 14 shows a comparison between the measured data and the pre-shot calculations for each experiment. The initial current rise matches calculation. However the calculation slightly over predicts the measured current peaks (~ 2.3 and ~ 1.7 MA) by a few percent indicating that some fine-tuning of the PHELIX transformer circuit model is in order. The current waveforms are sufficiently close to the $0.8x$ and $0.6x$ design so as to achieve the mixed and solid release states.

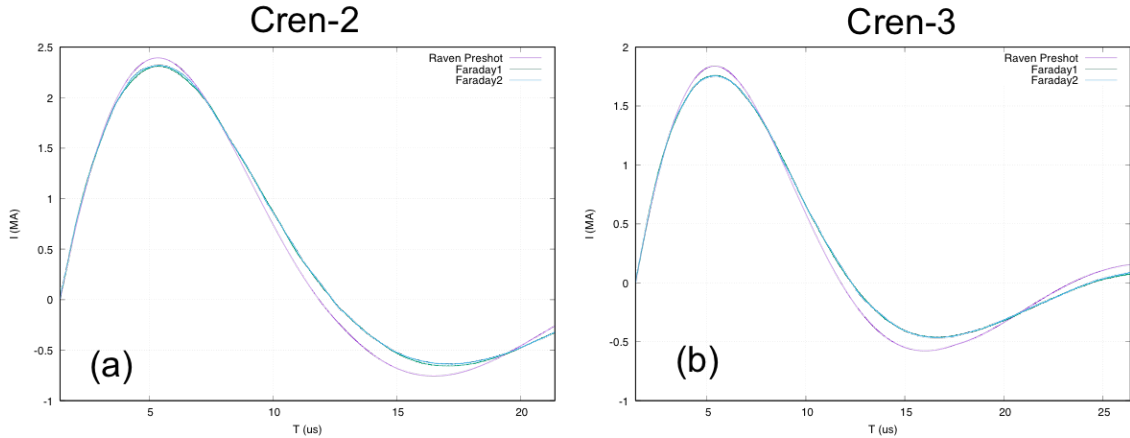


Figure 14 . Faraday rotation load current for (a) Cren-2 and (b) Cren-3 compared to pre-shot calculations.

Twenty-one proton radiograph movies were captured for each experiment. Figure 15 shows the static image of the tin target cylinder with three sectors of single mode perturbations ($kA = 0.1, 0.2$, and 0.3) on the inside surface. Also visible are evacuation holes in the upper glide plane. For Cren-2 a liner impact velocity was measured at 1.5 km/s. This equates to a shock pressure in the tin cylinder of ~ 20 kbar. The image shows fluid-like RMI growth of the three sectors. For Cren-3 the liner impact velocity was measured to be 1.0 km/s which translates into a ~ 10 kbar shock in the tin. This is below the release to solid-state threshold. It is observed that the RMI growth, while present, is much inhibited due to strength of the material. Both these results are qualitatively consistent with the pre-shot calculations. An additional feature observed in both experiments is density depressions due to cavitation/spallation in the bulk of the cylinder due to release from the outside surface as was predicted in the pre-shot calculations.

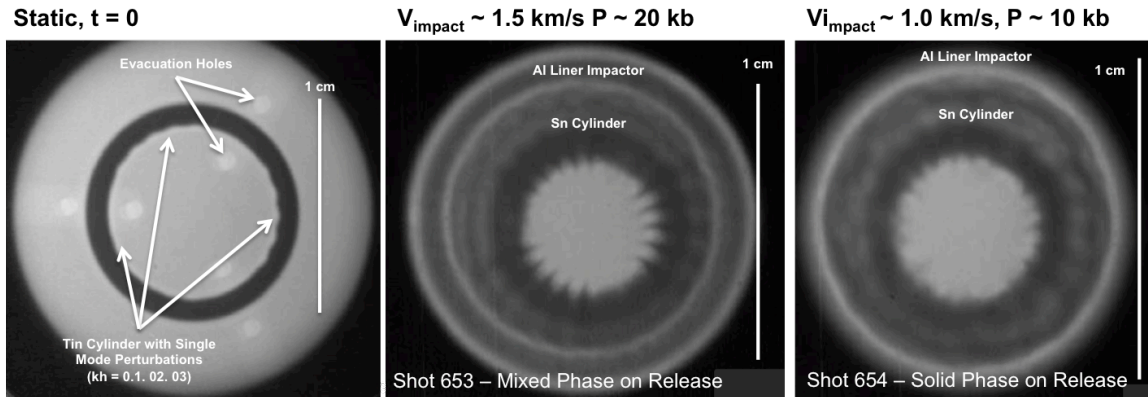


Figure 15. Static and dynamic proton radiographs of the Cren-2 and 3 experiments.

Detailed quantitative analysis of the RMI growth is currently underway and will be compared to calculations.

Summary

In partial fulfillment of the LANL Science Campaign-1 L2 Milestone (#5721), two PHELIX driven Crenulation experiments have been conducted at the LANSCE proton radiography facility in FY17 and documented in this report.

A synopsis of the experimental accomplishments is:

- New PHELIX load cassette to beam pipe interface was engineered and deployed
- Cren-2 and 3 experiments conducted at pRad on 29 November and 1 December
- 100 percent data return for both experiments
- No collateral damage to PHELIX or pRad facility
- Fastest turn around for PHELIX experiments ~2 days

The data will be used to validate EOS and strength models in LANL ASC Lagrangian Applications Project Flag code.

ⁱ J. Fung, et al., “Ejecta Modeling in the FLAG Hydrocode,” LA-UR-08-3835.

ⁱⁱ W. T. Buttler and M. B. Zellner, “Tin Ejecta Data Review: Toward a Statistical Material Fragmentation Model.” LA-UR-07-6522.

ⁱⁱⁱ W. T. Buttler et al., “Unstable Richtmyer-Meshkov Growth of Solid and Liquid Metals in Vacuum,” *J. Fluid Mech.*, **703**, 60-84, 2012.

^{iv} C. Greef, E. Chisolm, D. George, “SESAME 2161: An Explicit Multiphase Equation of State for Tin,” LA-UR-05-9414.

^v T. Canfield and T. Carney, private communication.

^{vi} L. G. Margolin and M. J. Andrews, “Models for Crenulation of a Converging Shell,” *Transactions of the ASME*, **136**, 084501-4, 2014.

^{vii} P. J. Turchi, *IEEE-TPS* **34**, 1919-1927, 2006.